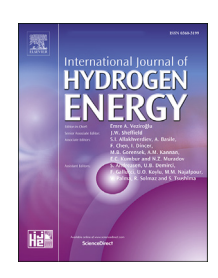


Available online at www.sciencedirect.com

ScienceDirect

journal homepage: www.elsevier.com/locate/he



Detecting hydrogen concentrations during admixing hydrogen in natural gas grids



Huib Blokland ^a, Jörgen Sweelssen ^b, Tommy Isaac ^c, Arjen Boersma ^{b,*}

- ^a TNO, Leeghwaterstraat 44, 2628 CA, Delft, the Netherlands
- ^b TNO, HTC 25, 5656 AE, Eindhoven, the Netherlands
- ^c Progressive Energy, Swan House-Bonds Mill Estate, Stonehouse, Gloucestershire, GL10 3RF UK

HIGHLIGHTS

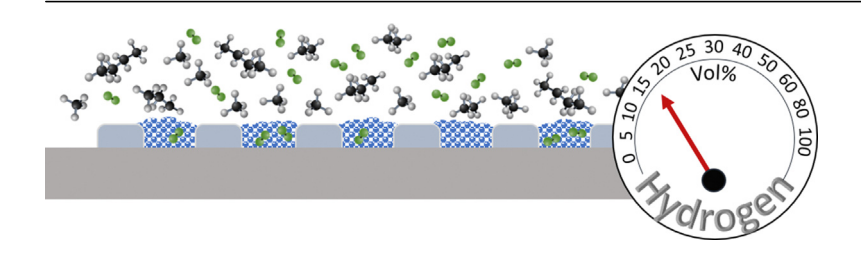
- A platinum based hydrogen sensor was developed showing full reversibility.
- It operated at room temperature without any hysteresis.
- Hydrogen detection in natural gas was demonstrated between 0.1 and 30 vol%.
- The hydrogen sensor can be easily combined with a full gas composition sensor.

ARTICLE INFO

Article history:
Received 7 May 2021
Received in revised form
24 June 2021
Accepted 26 June 2021
Available online 5 August 2021

Keywords:
Hydrogen admixing
Low cost sensor
Natural gas grid
Interdigitated electrodes
HyDeploy

GRAPHICAL ABSTRACT



ABSTRACT

The first applications of hydrogen in a natural gas grid will be the admixing of low concentrations in an existing distribution grid. For easy quality and process control, it is essential to monitor the hydrogen concentration in real time, preferably using cost effective monitoring solutions. In this paper, we introduce the use of a platinum based hydrogen sensor that can accurately (at 0.1 vol%) and reversibly monitor the concentration of hydrogen in a carrier gas. This carrier gas, that can be nitrogen, methane or natural gas, has no influence on the accuracy of the hydrogen detection. The hydrogen sensor consists of an interdigitated electrode on a chip coated with a platinum nanocomposite layer that interacts with the gas. This chip can be easily added to a gas sensor for natural gas and biogas that was already developed in previous research. Just by the addition of an extra chip, we extended the applicability of the natural gas sensor to hydrogen admixing. The feasibility of the sensor was demonstrated in our own (TNO) laboratory, and at a field test location of the HyDeploy program at Keele University in the U.K. © 2021 The Author(s). Published by Elsevier Ltd on behalf of Hydrogen Energy Publications LLC. This is an open access article under the CC BY license (http://creativecommons.org/licenses/by/4.0/).

E-mail address: arjen.boersma@tno.nl (A. Boersma).

^{*} Corresponding author.

Introduction

The energy transition from fossil to renewable sources is a major challenge in the coming decades. It is generally acknowledged that gas will play a major role in this transition replacing coal and oil for zero and low CO2 emitting fuel sources. This gas can have the form of natural gas, biogas, LNG, hydrogen or mixtures. The type and rate of transition will depend on the dominant fuel source in the country or region considered. Countries already having an extended natural gas infrastructure are considering the admixing of biogas or hydrogen to the natural gas. Or alternatively, replacing natural gas fully by hydrogen. A logical first step in the gas transition from carbon based fuel gasses to hydrogen is the admixing of hydrogen in an existing gas grid to replace part of the gas by hydrogen [1-4]. For a full green transition, this hydrogen will be preferably produced by electrolysers driven by wind turbines or solar power, however production methods utilising carbon capture and storage will likely prevail initially due to their much lower relative cost. For example, the Dutch gas network has great potential for the transport and distribution of natural gas containing a high concentration of hydrogen [5-8]. Furthermore, pilots across Europe have shown that percentages of hydrogen of up to 20 vol% in natural gas are no showstoppers for most end users [9-11]. The composition of the natural gas into which hydrogen will be blended will show greater variation in the future due to the increasing use of biogas and LNG. Therefore, in addition to the percentage of hydrogen, the other components should also be accurately measured. In order to be able to supply gas with sufficient security of supply and reliability, even when high concentrations of hydrogen gas are added, it is necessary for the network operators to measure gas quality at many locations, such as:

- At the point of injection into the network (check for desired percentage of hydrogen).
- In the distribution network (monitoring quality, possible billing of energy in the future).
- Hydrogen/natural gas separation (quality control of pure hydrogen or pure natural gas).
- Quality control at industrial end users.

This requires large numbers and affordable sensors for measuring the quality of hydrogen/natural gas mixtures. Currently, there is no cost-effective technology available for sufficiently reliable measurement of the composition and calorific value of natural gas/hydrogen mixtures. Some larger sensor concepts for hydrogen content detection have been proposed [12–15]. Smaller sensor solutions based on material interactions between hydrogen and an active material, such as metals, metal oxides or other nanomaterials have been discussed in the literature [16–19] A large variety of detection techniques was presented by Chauhan et al. [16], focusing on ppb level detection for safety applications, using thermal, electrochemical, electronic, mechanical, optical, or acoustic principles. A nice review of nanomaterials was given by Hu

et al. [17]. A general conclusion from many papers is the requirement of an elevated temperature for the optimal functionality of the sensor, and some of the nanomaterials showed a long response time of several minutes. In addition, the manufacturing of nanorod based sensors is very laborious and sensitive to defects. Many papers use catalytic metals such as platinum or palladium [18,19]. The hydrogen gas is absorbed into the metal and causes swelling or changes in electrical or optical properties. Only a few examples exist of platinum or palladium based capacitive hydrogen sensors [20,21]. Many of these solutions are limited in the hydrogen concentration range that can be detected and often show hysteresis in their response.

In this paper, we present the development of a small platinum based capacitive sensor that can be deployed in the gas grid for the monitoring of the hydrogen concentration, where no sampling is needed. In addition, based on previous developments of the gas sensor technology, the full gas composition can be assessed. The developments for hydrogen presented in the current paper are the continuation of the research on low cost gas sensors for natural gas that are based on small capacitive transduction elements [22–27]. The technology is protected by two patents, in which the characteristics of the technology is elucidated [22,23]. We will now briefly explain these developments leading to the application of the sensor technology for hydrogen.

A small interdigitated electrode is coated with a porous coating that will selectively absorb one or more components in a gas mixture. When more than one electrode is used, an array is obtained that will be able to measure multiple gases. The detection efficiency of this sensor array is highly dependent on the interaction of the target gases in the coatings that are applied to the interdigitating electrodes. The coatings must absorb/adsorb specific gases in a mixture and result in a change in the dielectric constant of the material. It is known that porous materials can adsorb significant amounts of gases on the inside surfaces of the pores. Polymer materials can absorb gases in the intrinsic porosity or free volume between the polymer chains. This adsorption and absorption is determined by the chemical and physical interactions with the surface of the porous material and is highly dependent on the pore sizes and surface chemistry. These interactions can be influenced by modifying the porous structure of the materials or the chemistry of the polymers. Coatings made from these materials are used to selectively absorb specific gases. The coating designed for hydrogen will be elucidated in the current paper, the coatings used for the hydrocarbons have been reported in previous publications [24-27].

Methods

The manufacturing steps for the hydrogen sensitive chip in the gas sensor array consist of 1) the manufacturing and packaging of the interdigitated electrodes on a silicon wafer; 2) the synthesis and application of the hydrogen coating formulation; 3) integrating the hydrogen sensing chip in the gas sensor array.

Sensing chips

Aluminum lines are manufactured on a silicon wafer using a process described before [26,27]. The line width and spacing is both 1 µm (Fig. 1A), and the total area of the electrodes is $700 \times 700 \mu m$, leading to an uncoated capacitance of about 5 pF. The chip is packaged in an LCC package (Fig. 1C) for connecting it to a PCB, to be connected to the read out electronics. This capacitance is measured using an AD7746 Capacitance-to-Digital converter chip (Analog Devices, Norwood, Ma, USA). A microprocessor converts the hexadecimal digital data to capacitance values that are exported to a PC using a USB connection. The 24-bits resolution lead to a resolution in capacitance of about 40 aF. Three physical sensors are also applied to the gas sensor PCB: temperature, pressure and thermal conductivity detector (TCD). The temperature and pressure are used to convert the data to values for concentration and partial pressure. The TCD (XEN-3880 Xensor Integration [28]) is used in some experiments to validate the capacitance readings.

Hydrogen sensing coating

Hydrogen is the smallest molecule in nature and can penetrate very easily into many materials, such as polymers, ceramics and even metals. For a sensor coating to be functional, it must selectively interact with hydrogen, and induce a change in material property. Since hydrogen is small, in many cases the molecules fit in the voids that are already present in the material, and thus do not give a change in any material property, other than weight. Examples are metal organic frame works or zeolites. Nevertheless, some materials are known to absorb hydrogen and expand or change conductivity, such as noble metals from the platinum group. The approach that was optimized in the present paper is the development of platinum nanoparticles in a porous metal oxide matrix. The exact details of the material and methods are presented elsewhere [23]. First highly porous titanium oxide sub-micron particles (approx. 300 nm) are synthesized from a titanium isopropoxide precursor in ethanol. In the pores of these titanium oxide particles, platinum nanoparticles (1-5 nm) are grown from a chloroplatinic acid precursor (Fig. 1B). After washing, a dispersion in water was obtained containing the platinum in ${\rm TiO_2}$ particles, suitable for deposition on the interdigitated electrodes. By means of manual deposition (e.g. micropipette) or automized printing, a droplet is applied to the square electrode area (Fig. 1C). After drying and curing at 80 °C, the electrodes are coated with a homogeneous layer of sensing material (Fig. 1D).

Chip integration

The hydrogen sensor chip as shown in Fig. 1 is integrated with the other gas sensing chips for hydrocarbons and physical sensors on a PCB (Fig. 2). As can be seen in Fig. 1, each chip has four electrode areas. Only two of those will be connected to the electronics, the other two are not used, and were added for design flexibility. This means that every chip has two channels for gas detection. Two sensor lay-outs were assessed: 1) bare PCB having five chips (i.e. ten channels), a temperature, pressure and TCD sensor (Fig. 2 left); 2) a packaged PCB (resulting from earlier sensor developments), having only four chips (eight channels) and a temperature and pressure sensor (Fig. 2 right). The 5-Chip sensor is used for the first validation of the hydrogen chip and TCD; the 4-Chip sensor was used in the field test, because this sensor was packaged and suitable for deployment in an actual gas pipe.

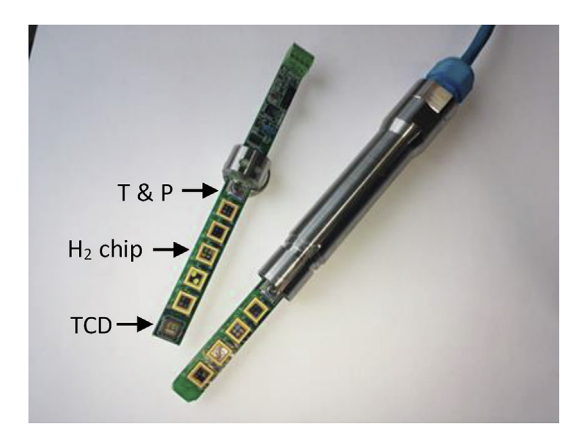


Fig. 2 – Integrated gas sensor array: (left) 5-Chip layout with temperature and pressure sensor and TCD; (right) 4-Chip layout with temperature and pressure sensor in a pressure resistant package.

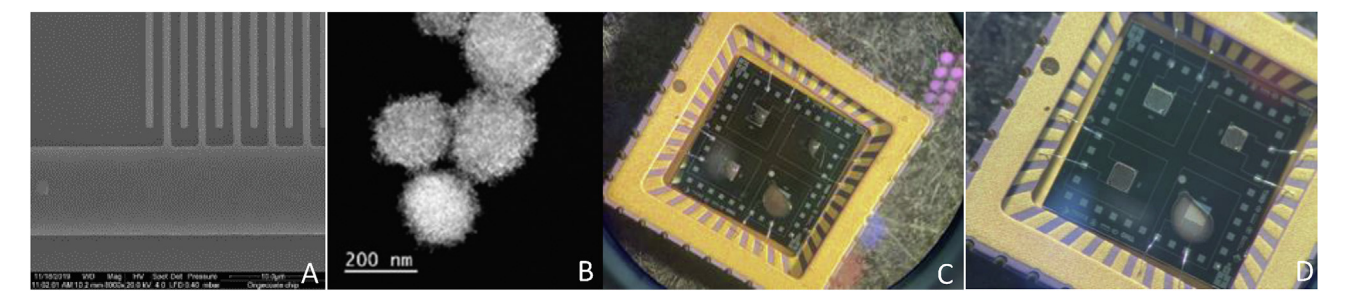


Fig. 1 — Coating the sensor chips: (A) Electron microscopy image of the comb electrode; (B) Electron microscopy image of titanium dioxide sensor particles; (C) drops of the hydrogen coating formulation applied to the four interdigitated electrodes; (D) Dried coating layer on the interdigitated electrodes.

The 4-Chip layout has been developed and validated for field tests [26] in which pressures can range between 1 and 10 bara, and for which an initial ATEX validation was drafted.

Exposure experiments

The sensor arrays that were manufactured, were exposed to various gas mixtures containing hydrogen, methane, ethane, propane, n-butane, iso-butane, n-pentane, iso-pentane, nitrogen and carbon dioxide using a gas exposure system that was described in other papers [26,27]. A series of 20 different gas mixtures was used to validate the sensor array in the laboratory setup. The pressure was set at 1.1 bara, and three temperature ranges were assessed: 10-12 °C; 24-26 °C; 44-46 °C. The exact temperature was not controlled, but changed during the experiments (±1 °C) as a result of fluctuating laboratory temperature and heating of the sensor electronics. The exact temperature was measured by the temperature sensor on the PCB and used in the correction of the sensor signals. The composition of the gas mixtures was regulated by flow controllers (Bronkhorst High Tech) and validated by the use of a gas chromatograph (Compact GC4.0, Global Analyser Solutions). The sensor array was calibrated using a selection of the gas mixtures (approx. 60 mixtures in total at the three temperatures). The relation between the setpoint gas concentrations and measured concentrations was established, and used for validating the feasibility of the gas sensor concept for gas mixtures having ten different gas components (including hydrogen). In the past, an array of eight channels was used for the calculation of six gases [24,25], now we use a similar array for ten gases. The first validation experiments will show if this extension of the sensor requirements will have negative consequences for its accuracy.

HyDeploy field test

Three of the 4-Chip gas sensors were deployed at the HyDeploy test site at the Keele University in the United Kingdom [9]. Hydrogen is produced in an electrolyser installed at a separate corner of the university campus (Fig. 3A). The supply line of the natural gas that is feeding the campus is diverted to this site, and the hydrogen is mixed with the natural gas at concentrations up to 20 vol%. The mixed gas is supplied to the campus, and is used in 30 university buildings and 100 residential sites. A boiler house for a residential block has central heating fueled by several gas boilers. The three gas sensors are positioned in the gas supply line of these boilers (Fig. 3B).

The gas composition during mixing is assessed using a gas chromatograph located at the other site of the campus, at distance of approx. 500 m. Since the use of gas fluctuated over time, but also over location on the campus (e.g. residential versus university buildings), there was a fluctuating time difference between the GC and sensor readings. This variation in time lag is compensated by using Dynamic Time Warping [29,30]. As will be shown below, the large fluctuations in hydrogen concentration, in combination with the fast response of the hydrogen sensor can be used to correlate the GC response to the sensor response. Dynamic Time Warping calculates the fluctuating time lag between two signals, by correlating these two signals using an adaptive time scale. A three weeks experiment was conducted at Keele. In the first week the sensors were calibrated and compared to the laboratory experiments. In the third week the gas composition was calculated using the calibration data of the first week. In the past, it was already noticed that the gas sensors need to be recalibrated after installation at a field test location. After the sensors are stabilized and calibrated in our laboratory, they show some drift of baseline during shipping: apparently the absorbing coatings absorb contaminants (including water) from the environment, that shift the sensor readings. Mitigation measures, such as longer preconditioning and airtight sealing, will be assessed in the future.

Theory of hydrogen adsorption

The capacitive sensor is designed to detect a change in capacitance of a coated interdigitated electrode. The change in capacitance is caused by a change in dielectric constant or resistivity of the coating that is applied to the electrode. In the past, we have assumed that the change in response is linear dependent on the gas concentration [24–27]. For most gas-





Fig. 3 – Keele university hydrogen production plant (A) and installed gas sensors in the supply line in a boiler house (B).

coating combinations, this approximation did not lead to too large errors. However, in the case of hydrogen, the response is not linear, and must be treated using an adsorption isotherm. Garcia Dieguez et al. [31] described the hydrogen chemisorption isotherms on platinum particles, and found that the adsorption of hydrogen can be described by a Langmuir isotherm for dissociative adsorption:

$$\theta = \frac{K\sqrt{P_{H_2}}}{1 + K\sqrt{P_{H_2}}} \tag{1}$$

 θ is the fraction of adsorption site that are filled with hydrogen, K is a adsorption constant and P the partial hydrogen pressure. The first experiment with the 4-Chip sensor at 25 °C is shown in Fig. 4A. We first assume that the dielectric constant or capacitance of the coating is linearly depend on θ . This hypothesis will be validated later. This means that when plotting 1/Cp (~1/ θ) versus 1/ $\sqrt{P_{\rm H2}}$, a straight line should be obtained. And, since the measured capacitance is done relative to an (arbitrary) off-set value, this off-set value needs to be corrected to obtain a straight line.

The lowest two points of Fig. 4C are omitted in Fig. 4D and the baseline is shifted with -0.3 pF to correct for the capacitance offset that was randomly chosen during sensor initiation. This plot indicates that the model can describe the response very well, at least for the higher hydrogen partial pressures. However, when looking at the lower concentrations, the error is quite substantial (Fig. 5).

Below partial pressures of 1 mbar, the difference becomes too large to allow reliable calculation of the hydrogen concentration (Fig. 5). Apparently at lower concentrations, a different adsorption mechanism is taking place. Recently, it was shown that hydrogen adsorbs onto platinum in two ways:

weakly bonded and strongly bonded [32,33]. So it may be possible to describe the hydrogen adsorption at low concentrations by another Langmuir isotherm. Or even by a more simple model, such as Henry adsorption. Since at higher concentrations, the adsorption does not behave linearly with partial pressure, we cannot use the linear matrix calculations that we have used so far for the calculation of the full composition. Therefore, the data processing for hydrogen is proposed as follows:

• For concentrations larger than 5 mbar, first the hydrogen pressure is calculated from the hydrogen chip only, using the Langmuir isotherm ($\beta K \sqrt{P/(1 + K \sqrt{P})}$). It will be

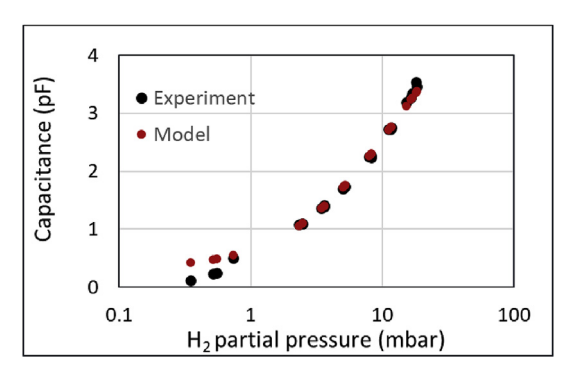


Fig. 5 — Measured (black) and predicted (red) capacitance versus hydrogen partial pressure. The graph is plotted logarithmically, to show the deviations at the lower concentration range. (For interpretation of the references to colour in this figure legend, the reader is referred to the Web version of this article.)

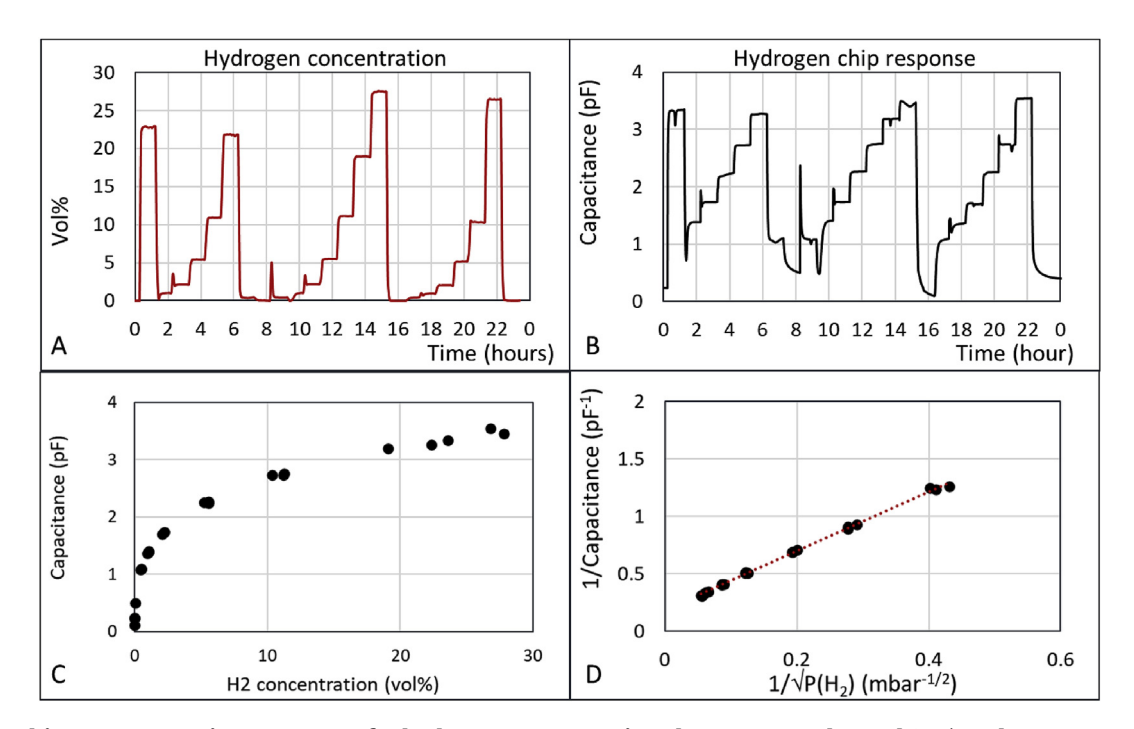


Fig. 4 - 4-Chip sensor experiment at 25 °C for hydrogen concentrations between 0 and 30 vol%. A) Hydrogen concentration versus time; B) Hydrogen chip response versus time; C) Capacitance versus hydrogen concentration; D) inverse plot of 1/Cp vs $1/\sqrt{P_{H2}}$.

apparent that the hydrogen concentration is larger than 5 mbar, when the chip response is larger than a critical value (~0.5 pF for the sensor of Figs. 4 and 5)

 For chip readings below 0.5 mbar, it is assumed that the response corresponds to βK√P.

Temperature dependency

In the hydrogen experiments it was observed that the response of the hydrogen chip is temperature dependent: the response increases with increasing temperature. This dependency can be described by a temperature dependent parameter K. Garcia Dieguez [31] introduces an Arrhenius dependency for the response parameters:

$$A(T) = A_0 e^{-Q \over RT} \tag{2}$$

In which A(T) is the temperature dependent response parameter, Q the activation energy, R the gas constant and T the temperature in K. All parameters in the equations are validated for this type of temperature dependency.

Data processing - high hydrogen concentration

The baseline shift that is required to optimize the fitting of the data to the Langmuir model as we have done in Fig. 4 needs to be assessed in an automated and reproducible way. First the measured capacitance is described by the relation:

$$C_{P} = \alpha + \beta \frac{K\sqrt{P_{H_2}}}{1 + K\sqrt{P_{H_2}}}$$
(3)

 α is the baseline off-set and β the capacitance correction factor relating gas adsorption to the change in actual dielectric constant and capacitance. This equation can be converted to:

$$C_{P} = \alpha + (\alpha + \beta)K\sqrt{P_{H_2}} - C_{P}K\sqrt{P_{H_2}}$$
(4)

Or

$$C_{P} = \kappa_{1} + \kappa_{2} \sqrt{P_{H_{2}} + \kappa_{3} C_{P} \sqrt{P_{H_{2}}}}$$
(5)

This equation can be solved using a least square approach of the high concentration hydrogen response results. The parameters κ that are derived include:

$$\kappa_1 = \alpha$$
 (6)

$$\kappa_2 = (\alpha + \beta)K$$
(7)

$$\kappa_3 = K$$
 (8)

For the assessment of all these relevant parameters, we have used four hydrogen sensors at three different temperatures. First, the fitting of the data revealed that all responses could be described by a single K parameter: $0.045 \pm 0.002 \, \text{mbar}^{-1/2}$. This value is subsequently used in the fitting of the other parameters α and β . The parameter α includes the off-set value of the sensor (C_0), that was arbitrary

chosen during manufacturing and the temperature dependent capacitance of the chips:

$$\alpha = C_0 + \alpha(T) = C_0 + \alpha_T e^{-Q\alpha/RT}$$
(9)

And the parameter β is the temperature dependency of the hydrogen concentration response:

$$\beta(T) = \beta_T e^{-Q\beta/RT} \tag{10}$$

The data processing starts with the plotting of the hydrogen chip response versus the hydrogen partial pressures for the three temperatures considered (Fig. 6A). The measurement points are fitted by a least square approach using Equation (3), and $K=0.045~{\rm mbar}^{-1/2}$ to obtain the values for α and β . The parameter C_0 , can be obtained by plotting α versus β . This is shown for the 4-Chip sensor in Fig. 6B. After correction the measured value of α by the value for C_0 , according to Equation (9), both α (T) and β (T) are plotted versus 1000/T as an Arrhenius plot, from which the activation energies can be calculated (Fig. 6C and D).

In Fig. 6C and D, the error bars for the temperatures and parameters α and β are indicated. The plot in Fig. 6B is almost linear in the temperature range between 11 and 45 °C. This would indicate that the values of $Q\alpha$ and $Q\beta$ are equal. This is confirmed by the plots in Fig. 6C and D, in which the slopes of the curves are almost equal (–1280 and –1330 K). This would lead to an average activation energy of the adsorption of hydrogen on platinum of 10.8 kJ/mol. This compares well with values between 8 and 9 kJ/mol that were presented by Pašti for adsorption on Pt/Pd surfaces [34].

Using the values for the parameters K, Q, Co, the parameters α_T and β_T can now be obtained from the measurement data. For the 4-Chip sensor presented in Figs. 4-6, these values are: α_T = 50.5 pF and β_T = 511 pF. These values depend on the nature of the TiO₂/Pt layer used for adsorbing hydrogen (layer thickness, concentration Pt, .), and the frequency of the AD chip. The AD chip that was used (AD7746) can use two frequencies (16 and 32 kHz), and the dielectric response of the coating depends heavily on this frequency. The parameters K and Q, remain constant, but the values of α_T and β_T change when switching from 16 to 32 kHz. The frequency used for the calculations in Figs. 4-6 was 16 kHz. When 32 kHz is used, the hydrogen response will be much lower. This phenomenon can be used to optimize the sensor for specific hydrogen concentration ranges. This is sometimes required for high hydrogen concentrations and high temperatures, as can be seen in Fig. 6A, where the 45 °C graph saturates at high hydrogen concentrations, caused by the saturation of the AD chip. These points are therefore not used in the data processing. An overview of all parameters are listed in Table 1 for four 4-Chip gas sensors used in this study. Sensor 1 was used in the data processing presented above. Sensors 2-4 are used in the HyDeploy field test.

The β_T parameter determines the height of the hydrogen response, and appears to be double for the 16 kHz when compared to the 32 kHz frequency. The ratio of α_T/β_T depends on the frequency of the AD7746 chip, and seems to be constant for a constant frequency.

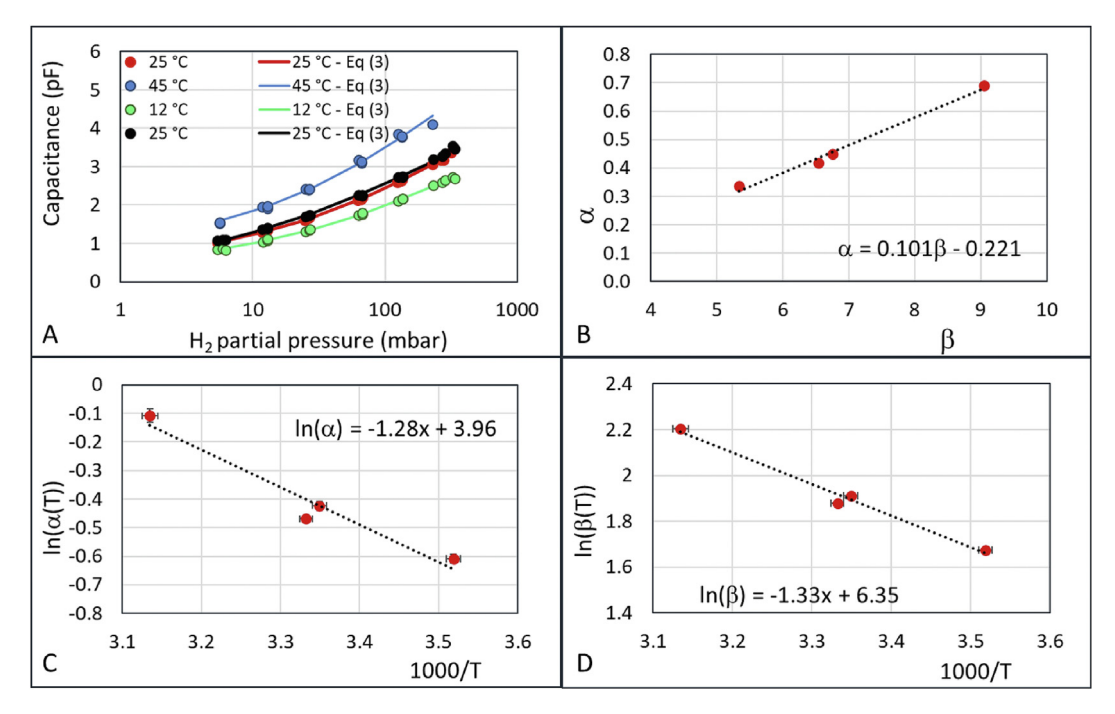


Fig. 6 — Data processing steps of the hydrogen chip response: A) Capacitance versus hydrogen partial pressure for one 4-Chip sensor at various temperatures, Equation (3) is fitted against the measurement point, resulting in values for α and β ; B) α is plotted versus β to obtain a value for C_0 ; C) C_0 in (α (T)) plotted versus 1000/T; D) C_0 0 in (C_0 1) plotted versus 1000/T.

Table 1 — Overview of all hydrogen chip parameters for four 4-Chip sensors assessed in the current study. Sensor 1 was used for the data protocol development as presented in Figs. 4—6. Sensors 2—4 are used for the deployment in the HyDeploy field test.

Parameter	Sensor 1	Sensor 2	Sensor 3	Sensor 4
f (kHz)	16	32	32	32
Co	-0.224 ± 0.01	-0.762 ± 0.01	2.83 ± 0.01	0.218 ± 0.01
$K \text{ (mbar}^{-1/2})$	0.045 ± 0.02	0.045 ± 0.02	0.045 ± 0.02	0.045 ± 0.02
Q (J/mol/K)	10.8 ± 0.2	10.8 ± 0.2	10.8 ± 0.2	10.8 ± 0.2
α_{T}	50.5 ± 2.0	13.3 ± 0.5	16.1 ± 0.8	15.5 ± 0.4
β_{T}	511 ± 11	262 ± 4	315 ± 4	306 ± 3
$\beta_{\rm T}/\alpha_{\rm T}$	10.1	19.8	19.5	19.7

Results

Sensitivity and response time of hydrogen sensing chip

The first assessment of the sensitivity of the hydrogen chip was performed by comparing the chip with the commercial TCD. The 5-Chip sensor was exposed to hydrogen in nitrogen, methane and natural gas, having a hydrogen concentration between 200 ppm and 20 vol%.

Fig. 7 shows that the sensitivity of the hydrogen chip is high at both high and low partial pressures. The TCD is especially sensitive at high partial pressures, but a lot less at low partial pressures. When looking at the signal-to-noise ratio and the resolution of the measuring equipment, a resolution of the hydrogen chip between 0.01 and 0.5 vol% can be expected, depending on the absolute value of the concentration. In addition, the hydrogen chip is a function of the partial pressure, but the TCD depends more on the concentration

than on the partial pressure. The hydrogen responses for the hydrogen chip are independent of the carrier gases and pressures and follow the same curve (Fig. 7B). This is not the case for the TCD, which clearly shows both a carrier gas and pressure dependency (Fig. 7C).

The exact response time of the sensor chip is difficult to measure, because in the gas mixing system the different gases are mixed and supplied through thin, long tubes. It is unknown when the gas reaches the sensors and whether the concentration changes occur as a step or gradually. In order to be able to make a statement, the response of the sensor chip was compared with the TCD. The TCD is known to react almost instantaneously when the gas composition changes, because it is a physical measurement of the gas. No diffusion processes are involved, other than in the mixing in the gas itself. Four concentration steps are shown in Fig. 8A, and one step is enlarged in Fig. 8B.

At a flow rate of 400 ml/min (which is approx. 1 volume of exposure cell/minute) the following is observed: 1) The start of

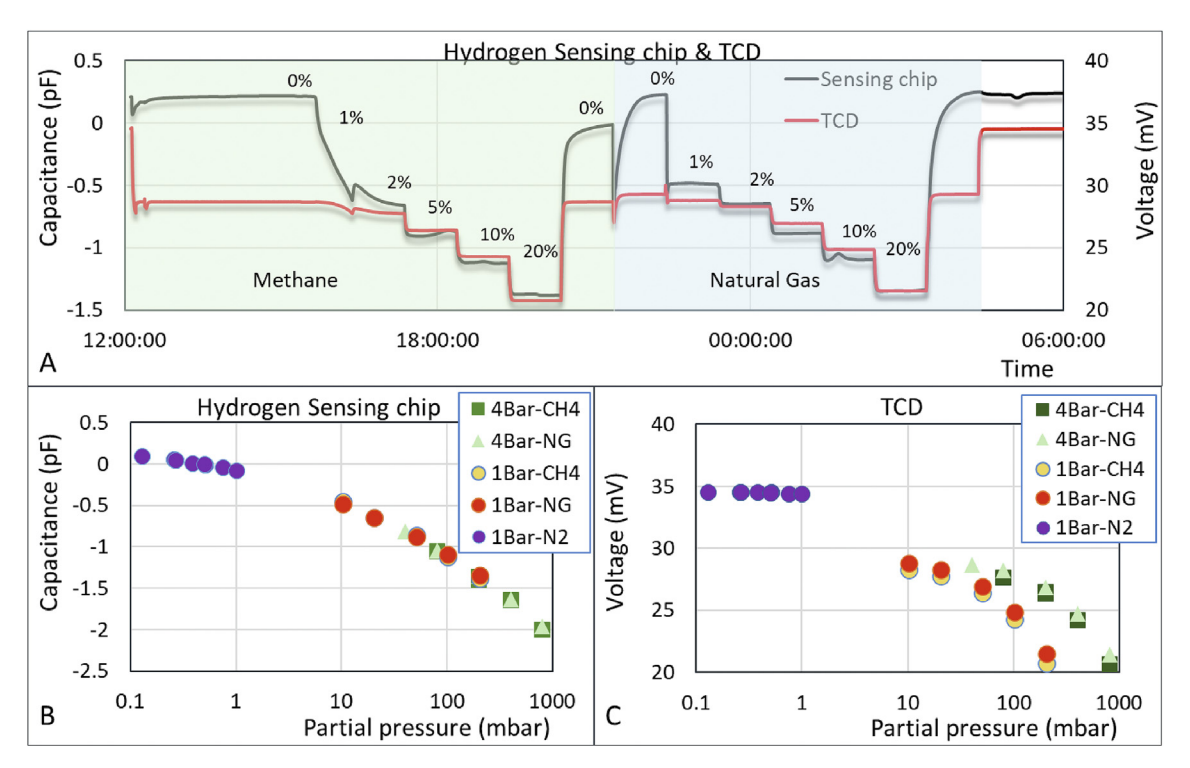


Fig. 7 — Response of the hydrogen chip and TCD on the 5-Chip gas sensor. A) Hydrogen concentrations between 0 and 20 vol % in methane and natural gas; B) Hydrogen chip response versus hydrogen partial pressure; C) TCD response versus hydrogen partial pressure.

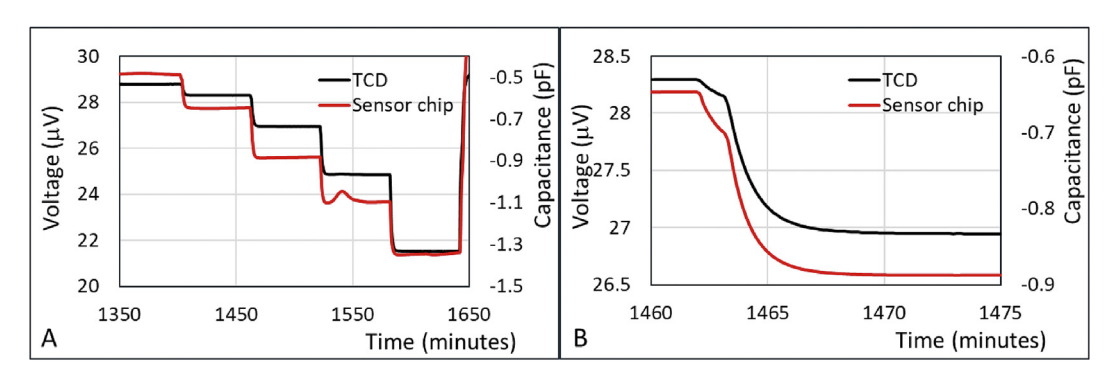


Fig. 8 - Hydrogen chip and TCD step responses for A) four steps (1-2-5-10-20 vol%); B) single step (2-5 vol%).

the response of the chip is 9 s faster than the TCD; 2) The 90% response is 190 s for the chip, and 220 s for the TCD; 3) The 95% response is 235 s for the chip, and 270 s for the TCD. This shows that the response of the chip is equal or even faster than the TCD. The response time therefore depends mainly on the flow and mixing of the gas, and not on the operation of the chip. So we can detect near instantaneous changes in hydrogen concentration.

Data processing of the hydrocarbon chips

The concentrations of the hydrocarbons in the mixtures are calculated using data protocols, which have already been published before [24–27]. The major difference with the previous approach is the number of chips that have been used. The 4-Chip sensors that have been used for laboratory and field test validation have eight sensing channels. Two of those

are used for the hydrogen chip, which leaves only six channels available for the assessment of the other nine gases in the mixtures. This could mean that the accuracy in the calculations could be lower than previously found. A second difference was the temperature corrections. In the data processing, an Arrhenius temperature dependency is introduced, similar to Equation (2). This temperature dependency is assessed simultaneously with the gas composition dependency, in the matrix calculations as explained by Sweelssen et al. [26] The calculated hydrogen and hydrocarbon concentrations are presented in the following sections.

Validation experiments

The data processing as described above was used to convert the sensor raw data into values for the hydrogen concentration in the gas mixtures. We used a single set of parameters for the entire temperature and concentration range that is used in the validation measurements. The results of one of the 4-Chip sensors (sensor 1 from Table 1) are presented in Fig. 9.

The Calorific Value (CV) and Wobbe Index (WI) of a gas mixture can be calculated from the composition of the gas and the individual calorific values of the components. The values of the calorific value and densities for the different gases as described in Table 2 are not according to ISO 6976, but are obtained from the NIST Webbook at a standard temperature of 15 °C and 1 atm. The calorific value of the gas is calculated by a linear addition of the contributions of all components in the gas. Compressibility is not taken into account.

The measured Calorific Value and Wobbe Index for the sensor are also plotted against the set-point values in Fig. 9.

Table 2 — Calorific values and densities of the gas components at the standard conditions 15 $^{\circ}$ C and 1 bar, derived from NIST Webbook [35].

Gas	Calorific value (MJ/m³)	Density (kg/m³)
Hydrogen	12.09	0.085
Methane	37.75	0.680
Ethane	66.55	1.283
Propane	95.28	1.899
n-Butane	125.95	2.544
Iso-Butane	125.02	2.533
n-Pentane	152.95	3.121
Iso-Pentane	152.24	3.113
Carbon dioxide	0	1.872
Nitrogen	0	1.185
Air	0	1.225

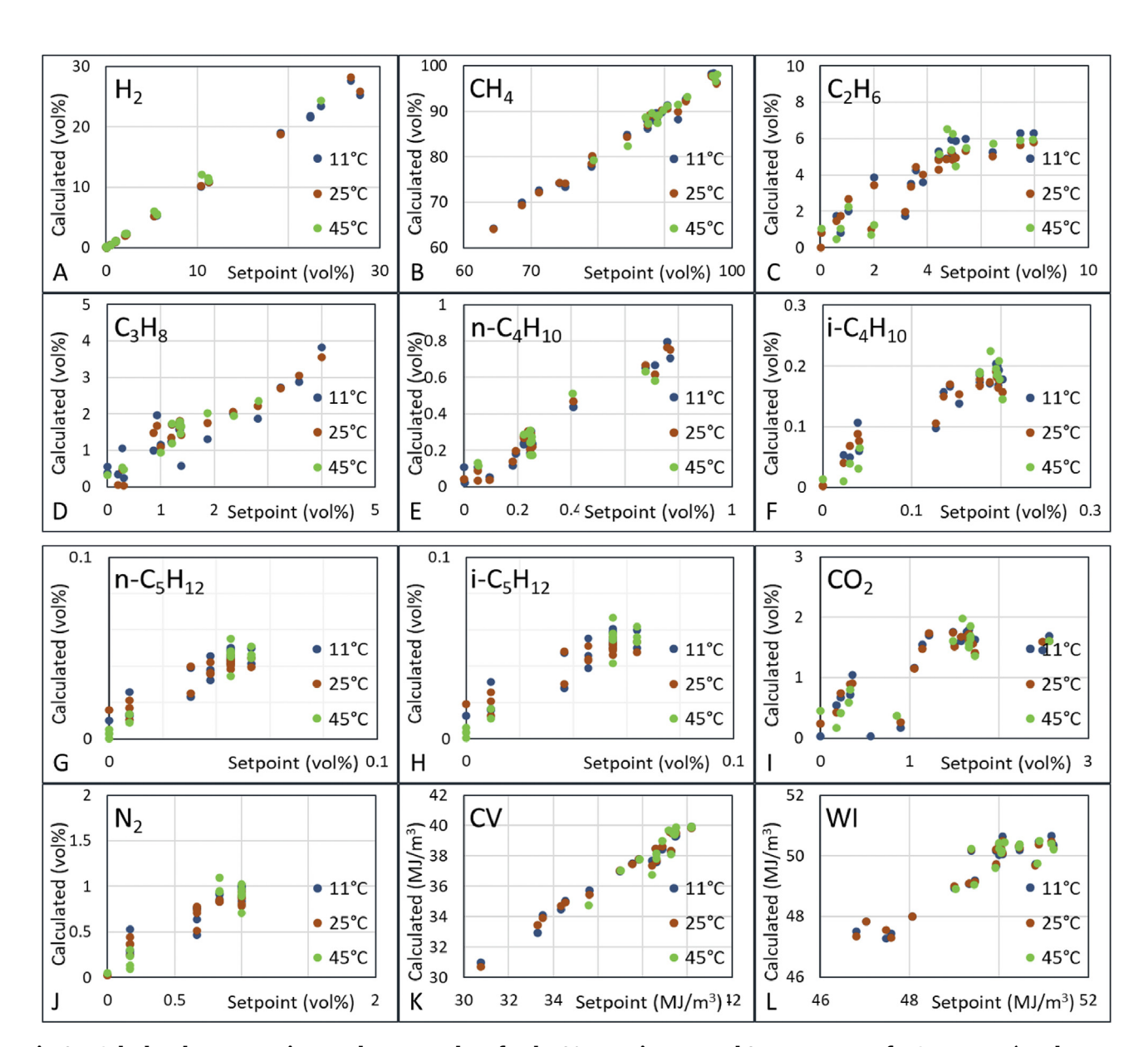


Fig. 9 — Calculated concentrations and energy values for the 20 gas mixtures and 3 temperatures for Sensor 1: A) Hydrogen; B) Methane; C) Ethane; D) Propane; E) n-Butane; F) iso-Butane; G) n-Pentane; H) iso-Pentane; I) Carbon Dioxide; J) Nitrogen; K) Calorific Value; L) Wobbe Index.

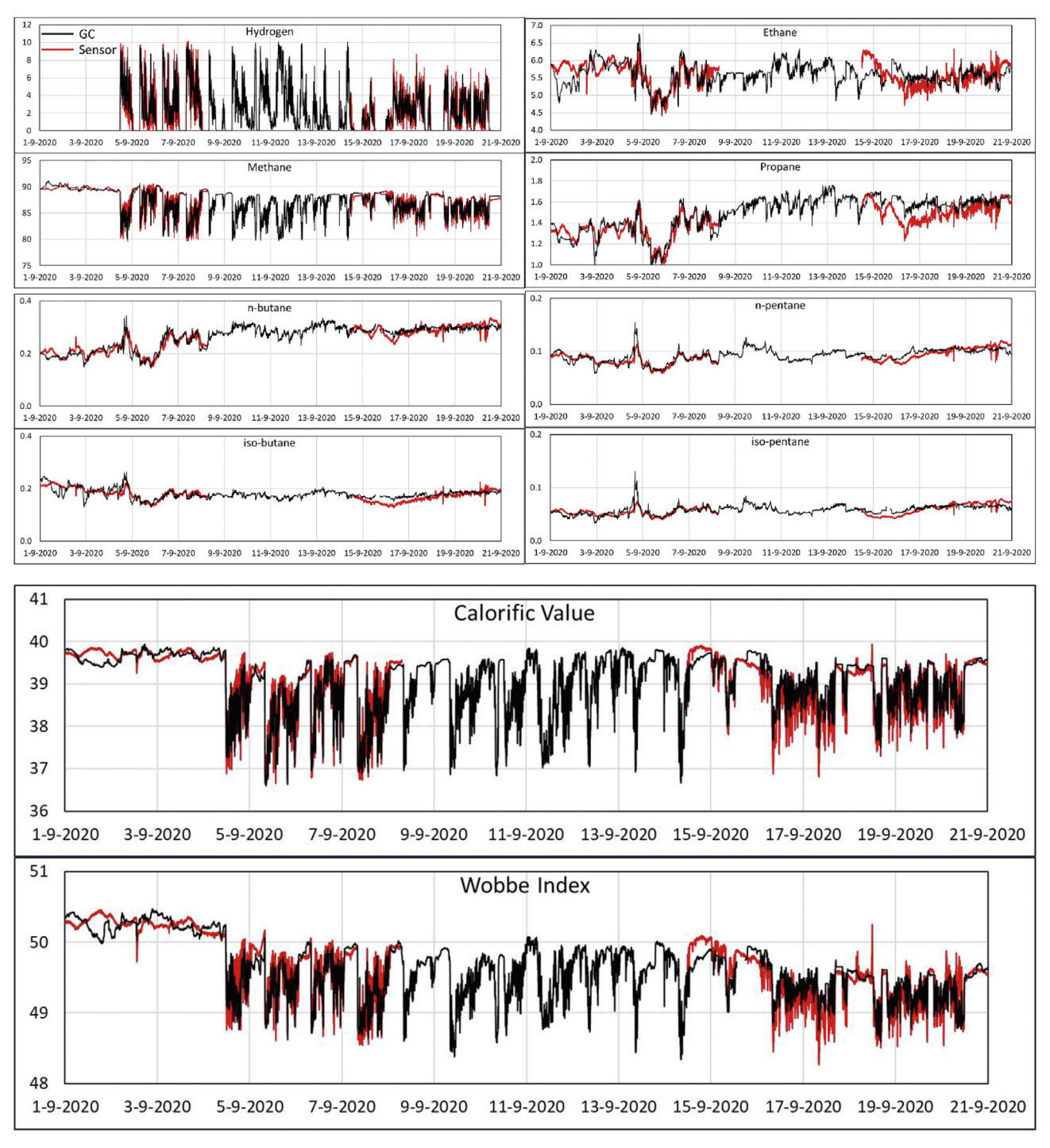


Fig. 10 — Gas concentrations and calculated energy parameters for the 4-Chip sensor (sensor 3) for 3 weeks in the HyDeploy field test. The first week (1—8 September) was used for calibration; the last week (14—21 September) was used for validation and comparison with the GC.

The Wobbe Index is calculated from the calorific value according to:

$$WI = \frac{CV}{\sqrt{\frac{\text{density_gas}}{\text{density_air}}}}$$
 (11)

The use of the values in Table 2 and the simplifications in the calculations of calorific value and Wobbe Index have no influence on the comparison of setpoint values with sensor values, because the setpoint values are also calculated in the same way.

The results presented in Fig. 9 show that for hydrogen and methane the correlation between GC setpoint and sensor results are very good for all temperatures. Most measurement points can be found on a single line, having a slope of 1. The accuracies of the higher hydrocarbons are much lower than

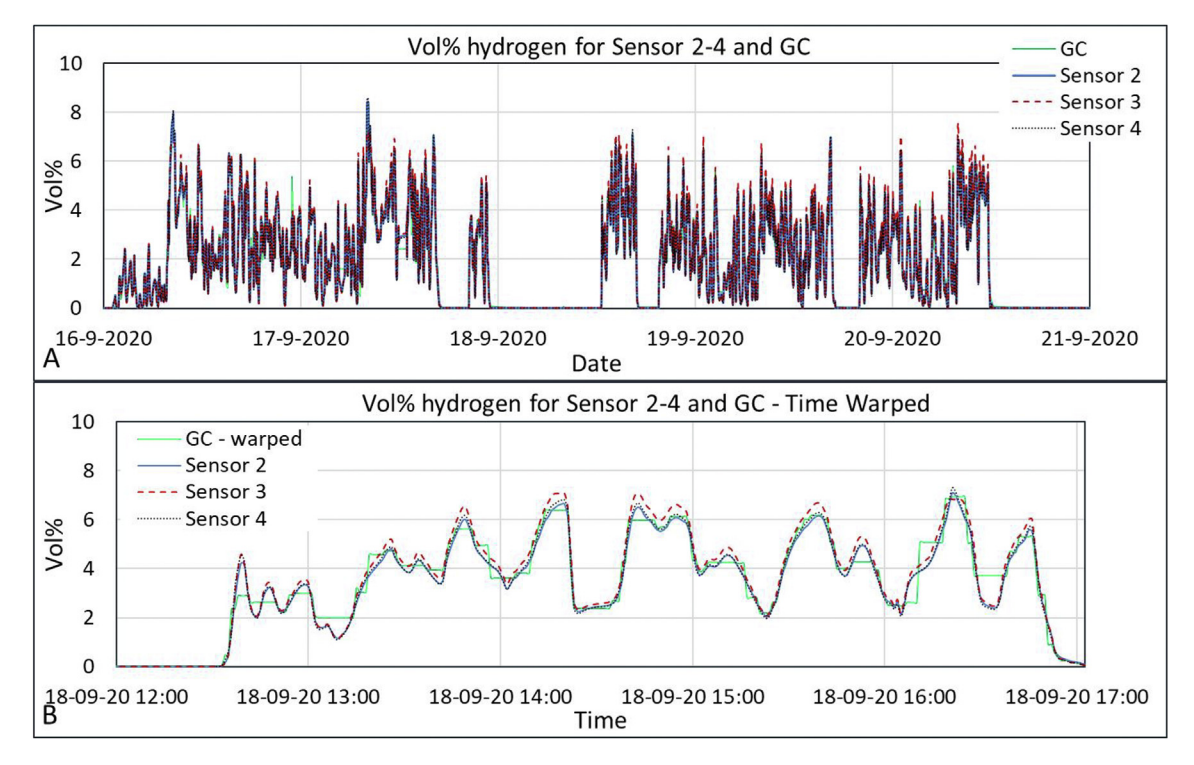


Fig. 11 — Reproducibility of the three hydrogen chips and GC for the third week of September: A) five days; B) zoomed in at 5 h of 18 September.

Table 3 $-$ Standard deviation between the GC data and the sensor 3 data for the third week in September.			
Gas	Standard deviation		
Hydrogen	0.37 vol%		
Methane	0.49 vol%		
Ethane	0.34 vol%		
Propane	0.11 vol%		
n-Butane	0.016 vol%		
Iso-Butane	0.016 vol%		
n-Pentane	0.008 vol%		
Iso-Pentane	0.007 vol%		
Carbon dioxide	0.52 vol%		
Nitrogen	0.74 vol%		
Calorific Value	0.25 MJ/m ³		
Wobbe Index	0.23 MJ/m ³		

hydrogen and methane. Part of this scatter of the higher hydrocarbons, carbon dioxide and nitrogen is caused by the use of only six channels for these nine gases. Some responses of gases are apparently too cross sensitive to be resolved by only six channels. This is especially the case for the higher hydrocarbons that can be differentiated with more difficulty, due to their comparable molecular structure. An additional reason for the lower accuracy, is the measurement time of only 1 h for each gas mixture. In case of larger concentration steps for some higher hydrocarbons, this hour stabilization time may be too short to obtain a stabilized signal. Nevertheless, overall, there is a clear correlation between setpoint values and measured values. The same holds for the calorific value and Wobbe Index. For the whole temperature range between 11 and 45 °C the measured points can be found scattered around

a line having slope of 1. These results showed sufficient correlation between setpoint values of the gas composition and sensor signals to deploy the sensors in a field test.

HyDeploy field test

The sensors 2-4 that are listed in Table 1 are deployed in the HyDeploy field test at the Keele University. After several weeks of exposure of the sensors in a natural gas flow, blending with hydrogen started in the first week of September 2020, following some equipment maintenance. This first week is used to assess the correlation between GC data and sensor data. As mentioned before, this type of coated electrode arrays requires some stabilization before use in a dry gas flow to remove all contaminants that have been adsorbed and absorbed by the coatings during shipping and installation. In addition, some baseline shift is sometimes observed between the laboratory testing of the sensor and the field deployment. For this reason, the sensors are recalibrated again during the first week of September when deployed in the gas grid. The gas composition values were used for this calibration of the GC that was stationed at approx. 500 m distance. As mentioned before, this distance introduced a varying time lag that was corrected for by Dynamic Time Warping. The results of the data processing for Sensor 3 are presented in Fig. 10.

Fig. 10 shows that the hydrogen fluctuations in the gas mixture can be very well measured using the gas sensor. For the hydrogen chip, the sensor parameters were used as shown in Table 1. Only the value for C_0 had to be slightly adapted during the first week of September. This shows that the response of the hydrogen chip is very stable and reproducible, and only a very small baseline shift must be compensated

between laboratory and field tests. This reproducibility is shown in Fig. 11A, in which the three hydrogen sensors (Sensor 2–4 from Table 1) are compared for the third week of September. The sensor traces for these five days fall exactly on top of each other. When zooming in on a few hours of September 18 (Fig. 11B), it can be seen that the sensors also match the GC values. However, since the GC was only taking one point in every 4 min, and the sensors ten points in every minute, part of the differences between GC and sensors, can be attributed to this difference in time scale.

Fig. 10 also shows the small fluctuations of the hydrocarbons can be very well measured using the 4-Chip gas sensors. The differences between calculated and measured concentrations are relatively small for most gases. This shows that some of the gas concentrations are correlated: e.g. the fluctuations in n-butane and i-butane follow a similar trend, as do the fluctuations in n-pentane and i-pentane. The correlation between GC values and sensor values is calculated as the standard deviation between the two. Table 3 shows both parameters for the gas concentrations and energy values. The largest values of the standard deviation (SD) are found for the non-calorific gasses carbon dioxide and nitrogen, indicating that the use of the 4-Chip sensor is not very suitable for an accurate detection of these two gases. The three gasses contributing the most to the calorific value: hydrogen, methane and ethane, also have the highest absolute inaccuracy. However, it must be stated that part of this difference is caused by the discrepancy between GC and sensor data rate. It is clear from Fig. 11, that during the period of the GC measurement (4 min), the hydrogen sensor reading can change significantly. This already introduces a significant error in the hydrogen concentrations. And since the hydrogen concentration is used to calculate all other components as well, this error is transferred to the other gasses.

The accuracy (SD) in Calorific Value and Wobbe Index is 0.64% (=0.25/39.0 MJ/m³) and 0.47% (=0.23/49.4 MJ/m³) respectively. This difference is mainly caused by the uncertainties in hydrogen, methane and ethane that have a standard deviation of more than 0.3 vol%.

Conclusions

The newly developed hydrogen chip has been shown to be very sensitive for the presence of hydrogen in gas mixtures. Laboratory experiments showed that the chip can measure hydrogen concentrations to at least 30 vol% having an accuracy of approx. 0.1 vol%. This was confirmed by the HyDeploy field test in which the hydrogen concentration admixed in natural gas was monitored for several weeks in a local gas grid at the Keele University in Newcastle-under-Lyme (U.K.). The calibration of the hydrogen chip was done in a controlled laboratory and most of the calibration parameters could be used during the field test. Only a small baseline shift was observed that could be caused by transportation and installation in the gas pipe of the gas grid. The three hydrogen sensors that were installed gave a very reproducible signal for the hydrogen concentration over the three weeks experiment. For the comparison of the sensor data with GC data that was obtained on a different location in the same network, Dynamic Time Warping

was used. The hydrogen concentrations followed the GC values very well. Furthermore, the hydrogen chip is very repeatable within the three weeks assessed. Unlike other platinum/palladium based hydrogen sensors, the porous coating absorbed and desorbed hydrogen very reversible, without changing the performance in time.

The hydrocarbon chips operated similar to the experiences of previous tests. These chips needed to be calibrated after installation. This calibration ensured the accuracy of methane to be approx. 0.5 vol%, ethane and propane 0.3 and 0.1 vol% respectively, and the higher hydrocarbons within 0.02 vol%. This combined accuracy resulted in an accuracy for the calorific value of 0.6% and for the Wobbe Index of 0.5%. In reality, these values will be better than this, because of the discrepancy between GC and sensor data acquisition.

Declaration of competing interest

The authors declare that they have no known competing financial interests or personal relationships that could have appeared to influence the work reported in this paper.

Acknowledgments

The research has been conducted as part of the TKI project SENSEH2GRID, funded by the "Topsector Energy" of the Dutch Ministry of Economic Affairs. The field demonstration was executed in cooperation with the HyDeploy program.

REFERENCES

- [1] Haeseldonckx D, D'haeseleer W. The use of the natural-gas pipeline infrastructure for hydrogen transport in a changing market structure. Int J Hydrogen Energy 2007;32(10):1381–6.
- [2] Walker SB, Lanen D van, Fowler M. Economic and environmental impact of using hydrogen enriched natural gas and renewable natural gas for residential heating. In: 4th IEEE international conference on smart energy grid engineering, SEGE; 2016. p. 215–20. 7589528.
- [3] Quarton CJ, Samsatli S. Power-to-gas for injection into the gas grid: what can we learn from real-life projects, economic assessments and systems modelling? Renew Sustain Energy Rev 2018;98:302—16.
- [4] Global S&P. https://www.spglobal.com/platts/en/marketinsights/blogs/natural-gas/051920-injecting-hydrogen-innatural-gas-grids-could-provide-steady-demand-the-sectorneeds-to-develop; 2020.
- [5] Giegler J, Weeda M. Contouren van een routekaart waterstof, topsector energie, maart. 2018.
- [6] The effects of hydrogen injection in natural gas networks for the Dutch underground storage. Report for the ministry of economic affairs; 2017. https://www.rvo.nl/sites/default/ files/2017/07/The%20effects%20of%20hydrogen%20injection %20in%20natural%20gas%20networks%20for%20the% 20Dutch%20underground%20storages.pdf.
- [7] Admissible hydrogen concentrations in natural gas systems, klaus altfeld and dave pinchbeck. GERG; 2017. https://www.gerg.eu/wp-content/uploads/2019/10/HIPS_ Final-Report.pdf.

- [8] Toekomstbestendige gasdistributienetten, Kiwa. July 2018. https://www.netbeheernederland.nl/_upload/Files/ Toekomstbestendige_gasdistributienetten_133.pdf?UA-142619432-2.
- [9] Isaac T. HyDeploy: the UK's first hydrogen blending deployment project. Clean Energy 2019;3(2):114–25.
- [10] HyBlend project: https://www.nrel.gov/news/program/2020/ hyblend-project-to-accelerate-potential-for-blendinghydrogen-in-natural-gas-pipelines.html.
- [11] Enbridge: https://www.enbridge.com/stories/2020/ november/enbridge-gas-and-hydrogenics-groundbreakinghydrogen-blending-project-ontario.
- [12] Hall JE, Hooker P, Jeffrey KE. Gas detection of hydrogen/ natural gas blends in the gas industry. Int J Hydrogen Energy 2020;46(23):12555–65. https://doi.org/10.1016/ j.ijhydene.2020.08.200.
- [13] Dörr H, Koturbash T, Kucherov V. Review of impacts of gas qualities with regard to quality determination and energy metering of natural gas. Meas Sci Technol 2019;30:022001.
- [14] Lantoine L, Ourliac M. Wobbe index measurement and control for industry: a mature technology facing new challenges. Int Gas Res Conf Proc 2017;1:49–57.
- [15] Hydrogen in the gas distribution networks. Australia: Department of Energy and Mining; 2019. http://www.coagenergycouncil.gov.au/sites/prod.energycouncil/files/publications/documents/nhs-hydrogen-in-the-gas-distribution-networks-report-2019_0.pdf.
- [16] Chauhan PS, Bhattacharya S. Hydrogen gas sensing methods, materials, and approach to achieve parts per billion level detection: a review. Int J Hydrogen Energy 2019;44(47):26076–99. https://doi.org/10.1016/ j.ijhydene.2019.08.052.
- [17] Hu K, Wang F, Shen Z, Yan Y, Liu H. Enhancement methods of hydrogen sensing for one-dimensional nanomaterials: a review. Int J Hydrogen Energy 2021;46(38):20119—38. https:// doi.org/10.1016/j.ijhydene.2021.03.117.
- [18] Sharma B, Myung J. Pd-based ternary alloys used for gas sensing applications: a review. Int J Hydrogen Energy 2019;44(57):30499-510. https://doi.org/10.1016/ j.ijhydene.2019.09.170.
- [19] Mirzai A, Yousefi HR, Falsafe F, Bonyani M, Lee J-H, Kim J-H, Kim HW, Kim SS. An overview on how Pd on resistive-based nanomaterial gas sensors can enhance response toward hydrogen gas. Int J Hydrogen Energy 2019;44(36):20552-71. https://doi.org/10.1016/j.ijhydene.2019.05.180.
- [20] Yamazaki H, Hayashi Y, Masunishi K, One D, Ikehashi T. A review of capacitive MEMS hydrogen sensor using Pd-based

- metallic glass with fast response and low power consumption. IEEJ Trans Sensors Micromachines 2019;138(7):312–8. https://doi.org/10.1541/ieejsmas.138.312.
- [21] Ratan S, Kumar C, Kumar A, Jarwal DK, Mischra AK, Upadhyay RK, Singh AP, Jit S. Room temperature high hydrogen gas response in Pd/TiO2/Si/Al capacitive sensor. Micro & Nano Lett 2020;15(9):632–5.
- [22] Snelders D, Boersma A, De Jong A-J. Gas sensor array and method. 2014, WO2016003272.
- [23] Boersma A, Sweelssen J, Blokland H, Van Ee R. Capacitive hydrogen sensor. 2019, WO2020175994.
- [24] Boersma A, Sweelssen J, Blokland H. Gas composition sensor for natural gas and biogas. Process Eng 2016;168:197–200.
- [25] Boersma A. Multiparameter Sensor Array for Gas Composition Monitoring. Proceedings 2018;2(867):2130867. https://doi.org/10.3390/proceedings2130867.
- [26] Sweelssen J, Blokland H, Rajamäki T, Sarjonen R, Boersma A. A versatile capacitive sensing platform for the assessment of the composition in gas mixtures. Micromachines 2020;11(2):116. https://doi.org/10.3390/mi11020116.
- [27] Sweelssen J, Blokland H, Rajamäki T, Boersma A. Capacitive and infrared gas sensors for the assessment of the methane number of LNG fuels. Sensors 2020;20:3345. https://doi.org/ 10.3390/s20123345.
- [28] Xensor integration, https://xensor.nl/products/thermalconductivity-gauge.
- [29] Müller M. Dynamic time warping. In: Information retrieval for music and motion. Berlin, Heidelberg: Springer; 2007. p. 69–82. https://doi.org/10.1007/978-3-540-74048-3_4.
- [30] https://medium.com/walmartglobaltech/time-seriessimilarity-using-dynamic-time-warping-explained-9d09119e48ec.
- [31] Garcia-Dieguez M, Hibbits DD, Iglesia E. Hydrogen chemisorption isotherms on platinum particles at catalytic temperatures: Langmuir and two-dimensional gas models revisited. J Phys Chem C 2019;123(13):8447–62.
- [32] Parker SF, Mukhopadhyay S, Jimenex-Ruiz M, Albers PW. Adsorbed states of hydrogen on platinum: a new perspective. Chem Eur 2019;25(26):6496—9.
- [33] Diaz-Morales O, Hersbach TJP, Badan C, Garcia AC, Koper MTM. Hydrogen adsorption on nano-structured platinum electrodes. Faraday Discuss 2018;210:301–15.
- [34] Pašti IA. Hydrogen adsorption on palladium and platinum overlayers: DFT study. Adv Electrocatal 2011. https://doi.org/ 10.1155/2011/305634. ID 305634.
- [35] NIST Webbook, https://webbook.nist.gov/chemistry/.